THE PUBLISHING HOUSE
OF THE ROMANIAN ACADEMY

PROCEEDINGS OF THE ROMANIAN ACADEMY, Series A,
Volume 21, Number 2/2020, pp. 163–172

ANALITYCAL APPROACH AND NUMERICAL METHODOLOGY VALIDATED AGAINST EXPERIMENTAL DATA ON S SHAPE AIRFOIL FOR WIDE FLOW ANGLES OF ATTACK

Adriana Sida MANEA[1], Sebastian MUNTEAN[2], Daniel Cătălin STROIȚĂ[1]

[1] "Politehnica" University of Timisoara, Bd. Mihai Viteazu 1, RO-300222, Timişoara
[2] Romanian Academy – Timisoara Branch, Bd. Mihai Viteazu 24, RO-300223, Timişoara
Corresponding author: Sebastian MUNTEAN, e-mail: seby@acad-tim.tm.edu.ro

Abstract. The paper presents O. Popa's analytical approach and the flow numerical methodology developed to determine the airfoil performances. Both methods are applied to determine the performances induced by flow over S shape airfoil for wide flow angles of attack (AoA). Also, the experimental investigations are conducted on S shape airfoil in the wind tunnel available at University Politehnica Timisoara. The pressure coefficient distribution on S shape geometry and the global coefficients (e.g. lift and pressure drag) are determined. Both theoretical and numerical results are compared against experimental data to assess their accuracy. As a result, the paper underlines the benefits and limitations of both analytical approach and numerical methodology to compute the flow over S shape airfoil and to predict the performances for wide flow angles of attack (AoA).

Key words: S shape airfoil, O. Popa's analytical approach, numerical methodology, experimental validation, wide flow angles of attack (AoA).

1. INTRODUCTION

The methods for the airfoil flow analysis have been summarized in several books [1,2], and the experimental results have been collected in catalogs such as [3,4]. In the last decades, the focus has switched from using available airfoil shapes and data toward numerical design and analysis their performances to met specifications for different applications [5–7]. These developments have been applied to both thin [8–10] and thick [11] air/hydrofoils. New challenges imposed in technical specifications for turbomachines require their operation over wide range angles of attack (AoA) and under direct and reverse flow conditions [12–14]. These requirements are fulfilled by S shape air/hydrofoils. However, both analytical approaches and numeric methodologies applied on S shape air/hydrofoils have to validate their results against experimental data for wide range AoA in order to assess their accuracy [15,16]. As a result, the tools developed based on these methods are checked providing the validity domain to be applied and the confidence level in the results.

This paper aims to assess the accuracy of the results obtained with both the analytical approach developed by Prof. O. Popa and the numerical methodology included in this paper against experimental data obtained on S shape airfoil for wide range AoA. The wind tunnel facility used to determine the aerodynamic performances of the airfoils is given in section 2. The setup associated to the S shape airfoil on the test rig and the flow regimes considered in the experimental investigation are detailed. The analytical approach developed by Prof. O. Popa is reviewed in section 3. The equations to compute the pressure coefficient over the profile and the lift coefficient are provided at the end of this section. The numerical investigations are performed based on the methodology developed in section 4. An overview of the numerical setup together with the considerations about the computational cases is presented. In section 5, both analytical solutions and numerical results are validated against experimental data considering the pressure coefficient over the airfoil as well as the global coefficients (e.g. lift and pressure drag), respectively. The flow investigations on S shape airfoil are performed for wide range AoA providing the benefits and the limitations of both analytical approach and the numerical methodology, respectively. The paper conclusions are summarized in section 6.

2. EXPERIMENTAL INVESTIGATIONS

The experimental investigations on the S shape airfoil have been performed on open loop wind tunnel [17]. Traditionally, the airfoils (e.g. NACA, Clark) are designed with a straight/arc mean chamber line over which a thickness distribution is added. Particularly, S mean camber line is selected for the S shape airfoils [18]. This type of airfoil is referred as two bi-directional airfoil shaped by Ma et al. [19]. The wind tunnel facility was designed by a group from University Politehnica Timisoara and Romanian Academy – Timisoara Branch (Fig. 1). It is manufactured from wood excepting the forked construction which is made by metal sheet. Two axial fans of 7.5 kW each are connected through forked construction ensuring a volumetric flow rate up to 14 m^3/s [20]. The velocity in the test section varies from 5 to 40 m/s whiles the range of the Reynolds numbers from $1.9 \cdot 10^5$ to $5.1 \cdot 10^5$, respectively. Air is sucked through the test section by both fans located at the rear of the tunnel. The test section with rectangular shape ($L = 1.5\,\text{m} \times B = 0.6\,\text{m} \times H = 0.3\,\text{m}$) is available on the rig (Fig. 2). A chamber with five strainers and a nozzle with a contraction ratio of 12:1 are installed upstream to the test section to reduce the flow turbulence and to increase the accuracy of the measurements.

S shape blade with a chord length of $l = 0.26$ m is installed in the test rig section as in Fig. 2. The leading edge is rounded with a radius of 15 mm while the trailing edge with 3 mm, respectively. The airfoil trunnion is positioned in the middle of the cord length $l/2 = 0.13$ m. The airfoil trunnion is located at 0.6 m with respect to the inlet surface of the test section. It is equipped with 46 pressure taps (23 on the pressure side (PS), 21 on the suction side (SS), 1 at the leading edge (LE) and 1 at the trailing edge (TE)), respectively. All taps are located in the middle of the blade high of $h = H/2 = 0.15$ m.

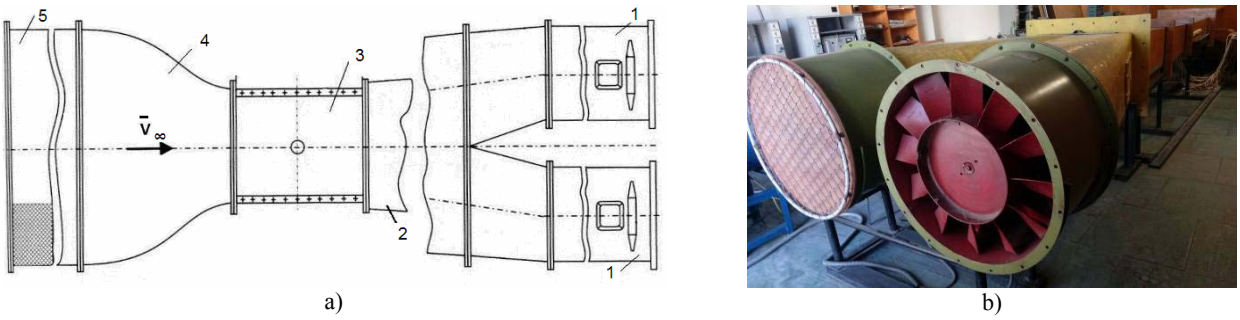

a) b)

Fig. 1 – The wind tunnel: a) sketch with main parts: 1 axial fans; 2 diffuser; 3 test section; 4 nozzle; 5 chamber with strainers; b) photo.

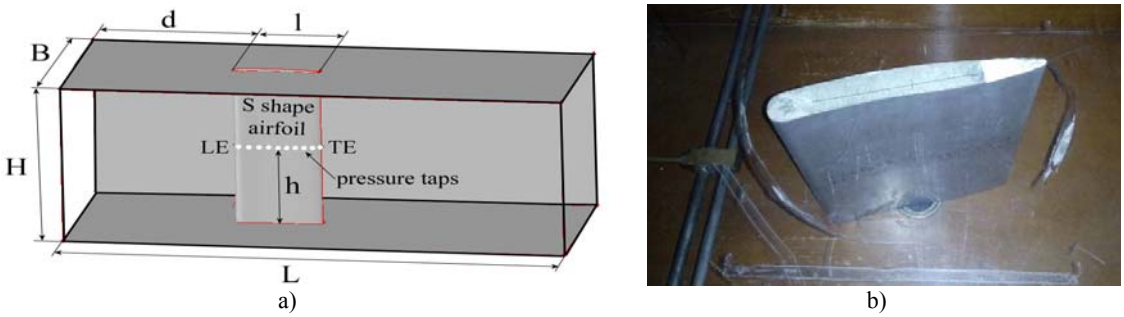

a) b)

Fig. 2 – The test section: a) sketch with S shape airfoil); b) photo.

The velocity and the turbulence level have been measured along to three survey axis located upstream to the test section using a DISA thermo anemometer and the hot wire probes with diameter of $d_f = 5\,\mu\text{m}$ and length of $l_f = 1.2$ mm, respectively. One can observe in Fig. 3 that both dimensionless velocity and the turbulence level remain constant along to 80% of the survey axis length. A deviation of the values up to 20% is obtained near to the boundary walls. The pressure on the airfoil is measured using a Scanivalve pressure transducer system with magnetic fluid. The Scanivalve sequentially connects each tap to the pressure transducer. The pressure coefficient (C_p) is determined using next equation:

$$C_{pi} = \left(p_i - p_\infty\right) \Big/ \left(\frac{\rho}{2} v_\infty^2\right), \tag{1}$$

where p_i is the static pressure measured in the taps located on the airfoil, v_∞ is the reference velocity, p_∞ is the reference static pressure and ρ is the air density. Both v_∞ and p_∞ values are measured along to the reference axis located at 0.25 m with respect to the test section inlet for each position of the airfoil using a Pitot-Prandtl probe.

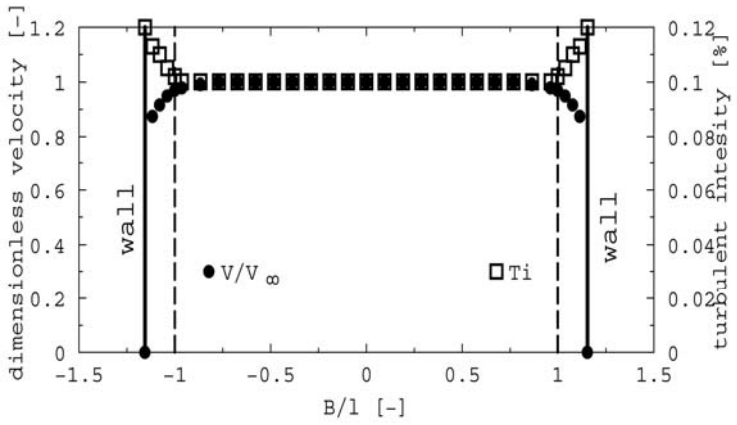

Fig. 3 – Velocity and turbulence intensity distribution measured along to the survey axis at the inlet of the test section.

The air moving over the airfoil produces a net force due to interaction between the fluid and the body. This net force is significantly influenced by the airfoil shape and AoA, respectively. The component of this net force perpendicular to the flow direction is called lift (A) while its component along the flow direction is called drag (D) – Fig. 4. The drag force is breaking in two parts: the pressure drag force (W) caused by the pressure distribution over the surface of the airfoil and the viscous drag force (F) generated by the friction in the boundary layer. The net force can be split in two components considering a different Cartesian system perpendicular and along to the airfoil cord (Fig. 4). As a result, both normal (N) and tangential (T) components are obtained.

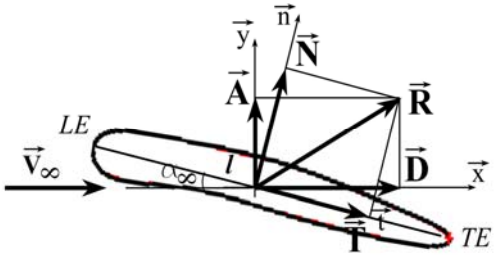

Fig. 4 – Forces on S shape airfoil.

Both lift coefficient C_A and pressure drag coefficient C_W are experimentally determined with:

$$\begin{aligned} C_A &= C_N \cos\alpha_\infty - C_T \sin\alpha_\infty, \\ C_W &= C_N \sin\alpha_\infty + C_T \cos\alpha_\infty, \end{aligned} \tag{2}$$

where $C_T = \left(\frac{1}{l}\right)\int_{\partial D} C_p \, \mathrm{d}y$ is the coefficient of the tangential component (T) and $C_N = -\left(\frac{1}{l}\right)\int_{\partial D} C_p \, \mathrm{d}x$ is the coefficient of the normal component (N) obtained as the integral on the contour of the S shape airfoil boundary (∂D). The experimental data measured for eight AoA (0°, ±5°, ±10°, ±15°, 25°) are presented in section 5. All coefficients determined based on experimental investigations are included in Table 2.

3. O. POPA'S ANALYTICAL APPROACH

O. Popa's approach leads to analytical solution solving of a plane, stationary and isochoric potential flow over an airfoil [21, 22]. Next equations can be defined

$$D^{ext} = (z) - D, \qquad \partial D^{ext} = \partial(z) \cup \left(-\partial D\right), \tag{3}$$

where D^{ext} belongs to a complex map (z), D is the inner field of an airfoil with unit length chord $l = 1$, the trailing edge $\zeta_B = 1$, the leading edge $\zeta_A = 0$, $D^{ext} \subset (z)$ is the outer field of the airfoil and $\partial D \subset (z)$ is it boundary.

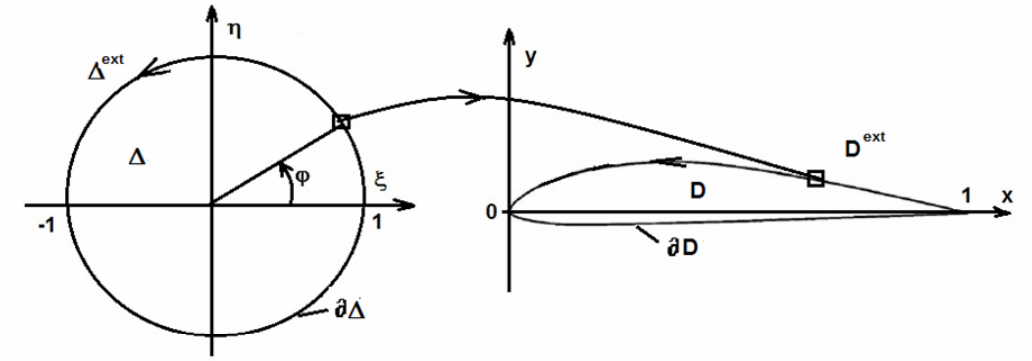

Fig. 5 – The conformal mapping of the external field of the unitary disc over the external field of an airfoil.

A conformal mapping function between the unit disc and the airfoil with unit cord length is defined by (4):

$$F : \Delta^{ext} \to D^{ext}, \quad z = F(z_*) = z(z_*), \tag{4}$$

considering the unit disc $\Delta \subset (z_*)$ with it centre in origin $O_* \in (z_*)$, the complex map origin (z_*), and the outer field of the disc $\Delta^{ext} = (z_*) - \Delta$ with boundary:

$$\partial\Delta^{ext} = \left(-\partial\Delta\right) \cup \partial(z_*). \tag{5}$$

This conformal function is holomorphic on $\Delta^{ext} \subset (z_*)$ and continuous over $\Delta^{ext} \cup \left(-\partial\Delta\right) \subset (z_*)$,

$$F \in C_z\left(\Delta^{ext}\right), \qquad F \in C^0\left(\Delta^{ext} \cup (-\partial\Delta)\right), \tag{6}$$

and asymptotically represented using a polynomial function with n degree,

$$\lim_{z_* \to \partial(z_*)} F(z_*) = f(z_*) = \sum\nolimits_{n=0}^{N} \left(B_n + i A_n\right) z_*^n, \quad A_n, B_n \in R, \tag{7}$$

the boundary $\partial D \subset (z)$ is the image $F_* : \Delta^{ext} \to D^{ext}$ of the circle $\partial\Delta \subset (z_*)$,

$$F(\partial\Delta) = \partial D, \quad \zeta_* = e^{i\vartheta} \in \partial\Delta \Rightarrow F(\zeta_*) = \zeta(\zeta_*) = \left[\xi(\zeta_*) + i\eta(\zeta_*)\right] \in \partial D \tag{8}$$

the relative abscissa and the relative ordinate of the boundary point $\zeta \in \partial D$ are presented as:

$$X(\varphi) \equiv \xi\left(\zeta_*\right)/l = \frac{1}{2}\left(1 + \cos\varphi\right), \quad Y(\varphi) \equiv \eta\left(\zeta_*\right)/l = \frac{1}{2}a_0 + \sum_{n=1}^{N}\left[a_n \cos(n\varphi) + b_n \sin(n\varphi)\right]. \tag{9}$$

The coordinates $X(\varphi), Y(\varphi) \in R$ are called relatives because they are related to the length $l \in R^+$ of the airfoil chord $D \subset (z)$. The coefficients $a_n, b_n \in R$ are defined as follows:

$$a_n = \frac{1}{\pi}\int_0^{2\pi} Y(\varphi)\cos(n\varphi)\,\mathrm{d}\varphi\,, \quad b_n = \frac{1}{\pi}\int_0^{2\pi} Y(\varphi)\sin(n\varphi)\,\mathrm{d}\varphi \quad (n=1,2,...)\,. \tag{10}$$

These coefficients are meeting Parseval's equation:

$$\frac{1}{2}\int_0^{2\pi} Y^2(\varphi)\mathrm{d}\varphi = \frac{1}{4}a_0^2 + \frac{1}{2}\sum_{n=1}^{N}\left[a_n^2 + b_n^2\right]. \tag{11}$$

The airfoil has the following parametrical representation:

$$X = \frac{1}{2}\left(1+\cos\varphi\right), \quad Y = \frac{a_0}{2} + \sum_{n=1}^{N}\left[a_n\cos(n\varphi) + b_n\sin(n\varphi)\right]. \tag{12}$$

In order to obtain the coefficients of the trigonometric polynomial function which approximate the airfoil: from $X = \frac{1}{2}\left(1+\cos\varphi\right)$ result the angle values $\varphi = \arccos(2X-1)$. We get the ordinate variation Y_p as an angles function, $Y=Y(\varphi)$, $\varphi\in[0,2\pi]$, $p=0,1,2\ldots(2N-1)$. Then, the trigonometric polynomial coefficients are yielded using these values:

$$a_n = \frac{1}{N}\sum_{p=0}^{2N-1} Y_p\cos\left(p\frac{n\pi}{N}\right), \quad b_n = \frac{1}{N}\sum_{p=0}^{2N-1} Y_p\sin\left(p\frac{n\pi}{N}\right). \tag{13}$$

The airfoil performances are determined using O. Popa's approach is done based on next equations:

$$X_{,\varphi} = \frac{\mathrm{d}X}{\mathrm{d}\varphi} = -\frac{1}{2}\sin\varphi\,, \quad Y_{,\varphi} = \frac{\mathrm{d}Y}{\mathrm{d}\varphi} = -\sum_{n=1}^{6} n\left[a_n\sin(n\varphi) - b_n\cos(n\varphi)\right], \tag{14}$$

with

$$N(\varphi) = -\sum_{n=1}^{6}\left[a_n\sin(n\varphi) - b_n\cos(n\varphi)\right], \quad N_{,\varphi} = \frac{\mathrm{d}N}{\mathrm{d}\varphi} = -\sum_{n=1}^{6} n\left[a_n\cos(n\varphi) + b_n\sin(n\varphi)\right]. \tag{15}$$

The velocity distribution (v) over the airfoil related to the upstream asymptotic velocity v_∞ is calculated with the following equation:

$$\frac{v}{v_\infty} = \overset{0}{V}(\varphi)\cos\alpha_\infty + \overset{1}{V}(\varphi)\sin\alpha_\infty\,, \tag{16}$$

where α_∞ is the angle of attack and the coefficients are given by equations (15):

$$\overset{0}{V}(\varphi) = -\frac{\sin\varphi - 2N_{,\varphi} + 2N_{,\varphi}(0)}{2\sqrt{X_{,\varphi}^2 + Y_{,\varphi}^2}}, \quad \overset{1}{V}(\varphi) = -\frac{1-\cos\varphi - 2Y_{,\varphi} + 2Y_{,\varphi}(0)}{2\sqrt{X_{,\varphi}^2 + Y_{,\varphi}^2}}. \tag{17}$$

The pressure coefficient (C_p) over the airfoil is given by next equation

$$C_p = 1 - \left(v/v_\infty\right)^2, \tag{18}$$

while the lift coefficient (C_A) is yielded using following equation:

$$C_A = C_{A0}\cos\alpha_\infty + C_{A1}\sin\alpha_\infty\,, \quad C_{A0} = -4\pi\sum_{n=1}^{6} n a_n\,, \quad C_{A1} = 2\pi\left(1 + 2\sum_{n=1}^{6} n b_n\right). \tag{19}$$

4. NUMERICAL METHODOLOGY

The two-dimensional computational domain corresponds with the test section available on test rig (Fig. 6). The geometry of the S shape airfoil is obtained using equations (12) with coefficients given in Table 1. Then, the geometry of the S shape airfoil is scaled down to the cord length of 0.26 m and 850 nodes are considered on the airfoil. A quadrilateral mesh with over 200k grid cells is considered for each case.

Table 1

The coefficients used to generate the geometry of the S shape airfoil

n	0	1	2	3	4	5	6
a_n	1.933903e-2	–4.919756e-3	–1.126427e-2	2.942869e-3	3.126620e-3	–1.869816e-3	6.832151e-4
b_n	0	6.432596e-2	–1.175604e-2	9.788755e-3	–6.176869e-3	3.844024e-3	0

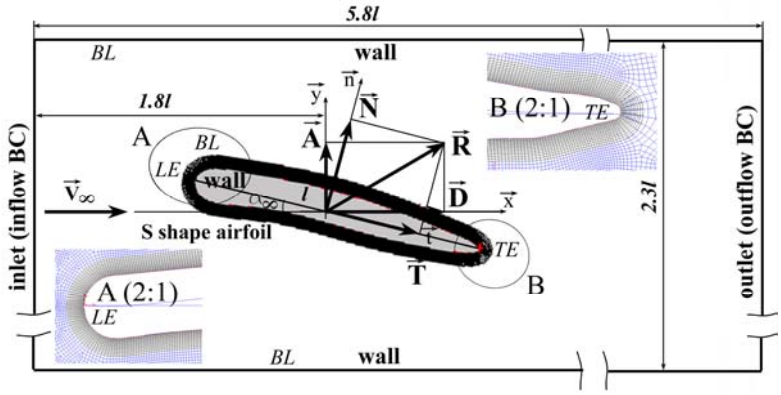

Fig. 6 – Computational domain, boundary conditions and mixed mesh.

One can observe that O type grid is generated around the airfoil to capture the velocity gradient within the boundary layer. Therefore, all grids are generated with $y+$ lower than 1. A grid dependency study is performed for each case to capture the flow separation region and the boundary layer transition.

The following boundary conditions are considered in the two-dimensional numerical simulations: (i) velocity components are imposed as inflow condition together with turbulent quantities. The reference velocity v_∞ considered for each case corresponds to the value measured on the test rig while other velocity component is negligible. Also, the turbulence intensity of 0.1% is imposed together with the turbulence length of 0.26 m corresponding to the cord length; (ii) solid boundary condition is implied on the airfoil, upper and lower walls and (iii) a gauge static pressure value is imposed as outflow condition.

The turbulent flow computation is performed using commercial codes [23, 24]. The Reynolds-Averaged Navier-Stokes (RANS) equations which describe the conservation of mass and momentum are solved using a finite volume method [25]. The Reynolds stress term in the momentum transport equations is solved using two equations k-ω SST turbulence model [26] implemented in Fluent V6.3 [23]. Also, four equations SST transitional turbulent model implemented in ANSYS/Fluent V16.2 [24] is considered in our investigations. The SST transitional model have used to compute the flow over the airfoil for cases where the k-ω SST model was not able to captured the boundary layer transition from laminar to turbulent. High (second or third) order schemes are considered for velocity, pressure and turbulence quantities. The steady computations are performed for small AoA while unsteady simulation for large ones, respectively. In all solutions, the residuals should be decreased by four orders of magnitude to converge the solution. The numerical investigations are performed considering the following flow AoA: 0°, ±5°, ±10°, ±15°, 25°. As a result, the pressure coefficient on the airfoil is determined based on equation (1). Then, the computed values are plotted against experimental data in next section. Both lift (C_A) and pressure drag (C_W) coefficients obtained based on numerical investigations are determined using next equations:

$$C_A = A \Big/ \left(\frac{\rho}{2} v_\infty^2 S \right), \quad C_W = W \Big/ \left(\frac{\rho}{2} v_\infty^2 S \right), \tag{20}$$

where A is the lift force on S shape airfoil, W is the pressure drag force, ρ is the air density, v_∞ is the reference velocity imposed on inlet section and $S = l \times 1$ is the reference area. The values obtained for all cases are included in Table 2.

5. ANALYTCAL AND NUMERICAL RESULTS AGAINST EXPERIMENTAL DATA

The analytical solutions and the numerical results are validated against experimental data over the S shape airfoil. The pressure coefficient obtained with equation (18) based on analytical approach is plotted with dashed line in next plots. The pressure coefficient numerically computed based on equation (1) is depicted with filled dots in the plots while the experimental data are marked with circles, respectively. Both analytical solutions and numerical results are compared against experimental data in next figure for eight AoA.

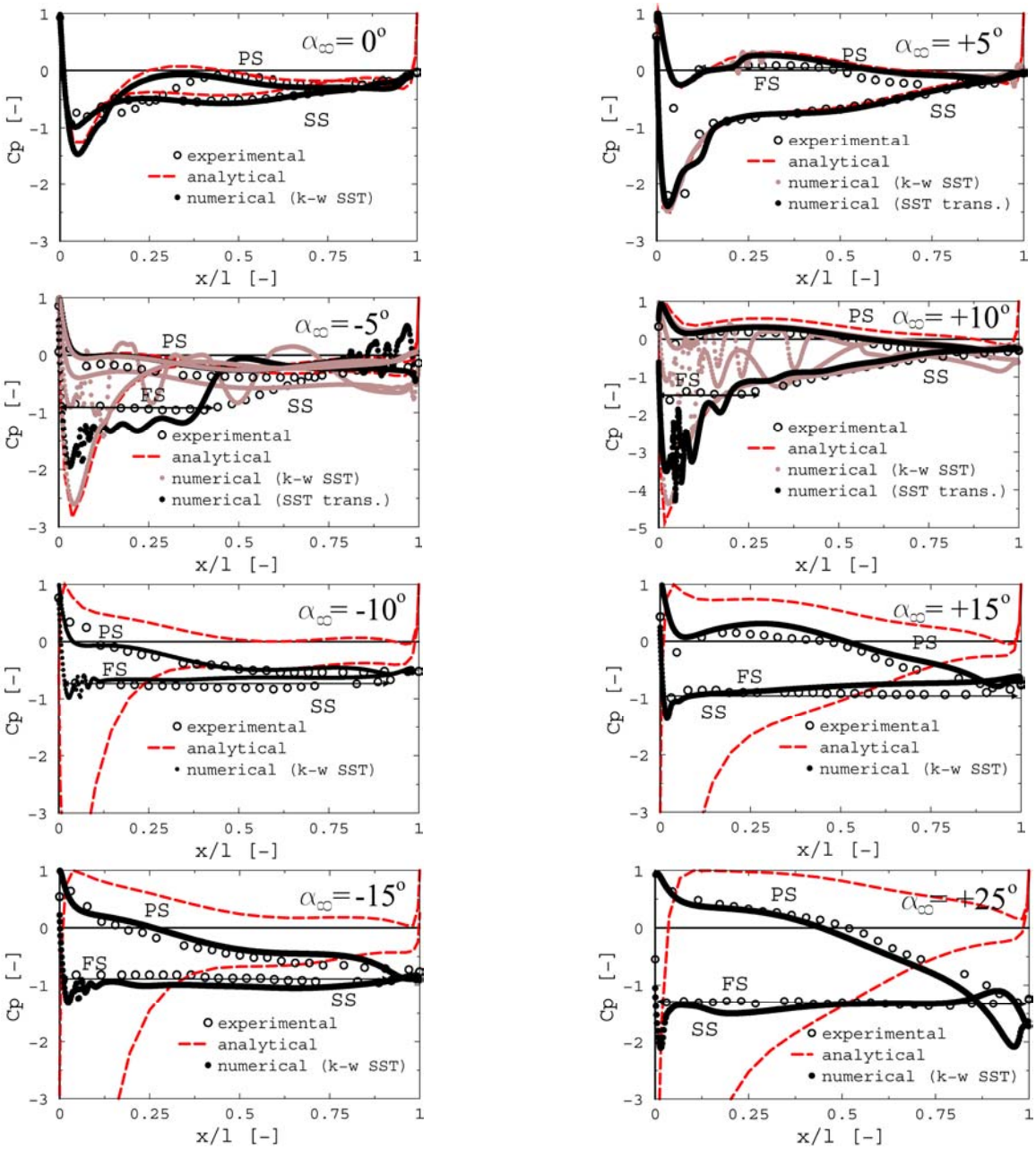

Fig. 7 – Pressure coefficient (C_p) vs. dimensionless cord length (x/l). The leading edge (LE) at $x/l=0$ and the trailing edge (TE) at $x/l=1$. Analytical solutions and numerical results validated against experimental data for eight AoA: $\alpha_\infty = 0°, \pm 5°, \pm 10°, \pm 15°, 25°$.

It is well know that the analytical solutions obtained with potential theory are valid if there is no flow separation. It is important to note that the analytical solutions determined on S shape airfoil capture quite well the experimental data for small AoA (0° and 5°) where small flow separation regions are developed. Contrary, the analytical solutions are not able to capture the experimental data when severe flow separation (FS) regions on the S shape airfoil are occurred.

The numerical results are able to reasonably capture the experimental data for all investigated cases. The numerical results are quite well for both small (0° and 5°) and large (–10°, ±15°, 25°) AoA. Bear in mind that the numerical solutions obtained for large AoA are unsteady. As a result, the numerical solutions depicted over the flow separation region correspond to a time snapshot. It can be seen in the flow separation region a sudden drop near to the leading edge of the pressure coefficient computed numerically with respect to the experimental data. This meaning that the flow in numerical simulation remains much longer attached on the airfoil. As a result, the flow separation is delayed in the numerical results with respect to the experimental data. The above statement explains why the lift coefficients computed numerically are larger than experimental ones (Table 2). Particularly, the numerical solutions obtained for AoA of –5° and 10° are limited to capture the flow separation zones (Fig. 7). Neither the k-ω SST two equations turbulence model nor the four equations SST transitional turbulence model is able to correctly capture the boundary layer transition from laminar to turbulent (Fig. 8). Moreover, both numerical solutions obtained in the separation region beyond the boundary layer transition point start to oscillate.

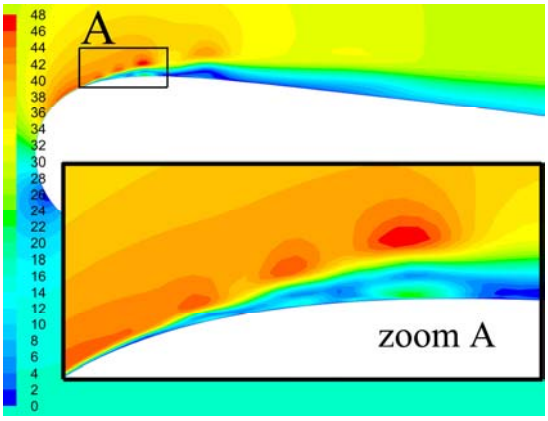

Fig. 8 – Velocity map near to the leading edge at AoA $\alpha = +10^{\circ}$.

Table 2

Analytical solutions and numerical results against experimental data

α [°]	Experimental data				Analytical results		Numerical results			
	C_N [-]	C_T [-]	C_A [-]	C_W [-]	C_A [-]	εC_A [%]	C_A [-]	εC_A [%]	C_W [-]	εC_W [%]
–15	–0.486	0.139	–0.434	0.260	-	-	–0.711	63.780	0.295	13.447
–10	–0.402	0.115	–0.376	0.183	-	-	–0.303	–19.341	0.145	–21.017
–5	–0.350	0.070	–0.343	0.101	–0.476	38.776	–0.534	55.572	0.0736	–27.106
0	0.161	0.0253	0.161	0.025	0.143	–11.180	0.108	–32.683	0.0192	–23.050
5	0.623	0.0818	0.613	0.136	0.761	24.144	0.755	23.223	0.0283	–79.189
10	0.859	0.072	0.834	0.220	-	-	1.150	37.918	0.0525	–76.148
15	0.680	0.0865	0.634	0.259	-	-	0.709	11.795	0.243	–6.267
25	1.177	0.0778	1.034	0.568	-	-	0.985	–4.705	0.505	–11.031

Both lift (C_A) and pressure drag (C_W) coefficients computed analytical and numerical are compared against experimental data in Table 2. Also, the relative deviation of each value is determined with respect to the experimental one using the following formulae:

$$\varepsilon_{\otimes} = \frac{(\otimes_{anal/num} - \otimes_{\exp})}{\otimes_{\exp}} \times 100 \ [\%], \tag{21}$$

The numerical values of the lift coefficient are larger than the experimental data due to the delay of the flow separation in the numerical solutions. Contrary, the pressure drag coefficient determined based on the numerical simulation is lower than the experimental data due the same reason.

6. CONCLUSIONS

The paper is focused on the flow over S shape airfoil to assess the accuracy of the analytical and the numerical results against the experimental data. The flow investigations were performed considering a wide range AoA from −15° to 25° with increment of 5°. The test rig available at University Politehnica Timisoara and the experimental setup were detailed. The pressure, lift and pressure drag coefficients are experimentally determined. Further, the analytical approach based on the conformal mapping method is described and applied to determine both pressure and lift coefficients on S shape airfoil. Next, the numerical methodology is developed to compute the turbulent flow over S shape airfoil. Then, the pressure, lift and pressure drag coefficients were numerically obtained. The pressure coefficients determined on S shape airfoil using both analytical approach and numerical results were compared against experimental data.

The analytical solutions obtained for small AoA (0° and 5°) are agreed quite well with experimental data due to small flow separation regions. The analytical approach based on conformal mapping method allows a relative simple and fast estimation of the performances on S shape airfoil. As a result, the analytical solutions are accurately enough at small AoA to be used in the design stage.

The experimental data were reasonably captured by the numerical results for all investigated cases. The numerical results are quite well for both small (0° and 5°) and large (−0°, ±15°, 25°) AoA. Particularly, the numerical solutions obtained for AoA of −5° and 10° are limited in order to accurately capture the boundary layer separation. Therefore, the numerical methodology can be applied to analyse the flow over S shape airfoil for wide range of AoA to determine its performances. However, the experimental data have to be used in order to validate the numerical results. Further investigations are focused to capture more accurate the boundary layer separation and the performances of the cascades with S shape airfoils.

ACKNOWLEDGEMENTS

Dr. Muntean S. was supported by Romanian Academy program.

REFERENCES

1. L. DRAGOŞ, *Mathematical methods in aerodynamics*, Kluwer Academic Press and Romanian Academy Press, 2003.
2. J. ROM, *High angle of attack aerodynamics*, Springer-Verlag, New York, 1992.
3. F. W. VON RIEGELS, *Aerodinamische Profile*, R. Oldenbourg, München, 1958.
4. D. ALTHAUS, F. X. WORTMANN, *Stuttgarter Profilkatalog I. Experiemental results from the laminar wind tunnel of the Institut für Aero- und Gasdynamic de Universität Stuttgart*, Friedr. Vieweg & Sohn, Braunschweig/Wiesbaden, 1981.
5. H. DUMITRESCU, V. CARDOS, N. ALEXANDRESCU, *Computation of separating laminar boundary-layer flows*, Proceedings of the Romanian Academy, Series A, **4**, *3*, pp. 151-156, 2003.
6. S. BERNAD, A. GEORGESCU, S.-C. GEORGESCU, R. SUSAN-RESIGA, I. ANTON, *Flow investigations in Achard turbine*, Proceedings of the Romanian Academy, Series A, **9**, *2*, pp. 129-140, 2008.
7. I. MOISĂ, R. SUSAN-RESIGA, S. MUNTEAN, *Pump inducer optimization based on cavitation criterion*, Proceedings of the Romanian Academy, Series A, **14**, *4*, pp. 317-325, 2013.
8. W. R. HAWTHORN, C. WANG, C. S. TAN, J. E. McCUNE, *Theory of blade design for large deflections: Part I – Two-dimensional cascade*, Journal of Engineering for Gas Turbines and Power, **106**, pp. 346-353, 1984.
9. R. SUSAN-RESIGA, S. MUNTEAN, S. BERNAD, T. FRUNZĂ, D. BALINT, *Thin hydrofoil cascade design and numerical flow analysis. Part I – Design*, Proceedings of the Romanian Academy, Series A, **7**, *2*, pp. 117-126, 2006.
10. R. SUSAN-RESIGA, S. MUNTEAN, S. BERNAD, T. FRUNZĂ, D. BALINT, *Thin hydrofoil cascade design and numerical flow analysis. Part II – Analysis*, Proceedings of the Romanian Academy, Series A, **7**, *3*, pp. 175-182, 2006.
11. T. FRUNZĂ, R. SUSAN-RESIGA, S. MUNTEAN, S. BERNAD, *Optimization of the hydrofoil cascade and validation with quasi-analytical solution for hydraulic machinery*, IOP Conf. Ser.: Earth Environ. Sci., **12**, p. 012075, 2010.
12. I. ANTON, V. CAMPIAN, I. CARTE, *Hydrodynamics of the bulb turbines and bulb pump-turbines* (in Romanian), Edit. Tehnică, Bucharest, 1988.

13. A. IOSIF, I. SÂRBU, *Numerical modeling of cavitation characteristics and sensitivity curves for reversible hydraulic machinery*, Engineering Analysis with Boundary Elements, **41**, pp. 18–27, 2014.
14. G. VENTURELLI, E. BENIN, *Kriging-assisted design optimization of S-shape supersonic compressor cascades*, Aerospace Science and Technology, **58**, pp. 275–297, 2016.
15. S.M.A. AFTAB, A.S. MOHD RAFIE, N.A. RAZAK, K.A. AHMAD, *Turbulence model selection for low Reynolds number flows*, PLoS ONE, **11**, *4*, e0153755, 2016.
16. D. LEE, T. NONOMURA, A. OYAMA, K. FUJII, *Comparative studies of numerical methods for evaluating aerodynamic characteristics of two-dimensional airfoil at low Reynolds numbers*, Int. J. of Computational Fluid Dynamics, **31**, *1*, pp. 57-67, 2017.
17. C.D. GALERIU, A.S. BUGARSCHI (MANEA), *Airfoil characteristics and flow parameters tested in a wind tunnel*, Proceedings of the Fourth Conference on Hydraulic Machinery and Hydrodynamics, **1**, pp. 19-26, Timisoara, Romania, 1994.
18. B. CHACKO, V. BALABASKARAN, E.G. TULAPURKARA, H.C. RADHA KRISHNA, *Performance of S-cambered profiles with cut-off trailing edges*, ASME Journal of Fluids Engineering, **116**, *3*, pp. 522-527, 1994.
19. P.F. MA, J. WANG, H.F. WANG, *Investigation of performances and flow characteristics of two bi-directional pumps with different airfoil blades*, **61**, 10, pp. 1588-1599, 2018.
20. C.D. GALERIU, *Potential flows and hydrodynamic approach of the hydrofoil cascades. Boundary layer theory* (in Romanian), IPTVT, **1**/**2**, Timisoara, 1984/1986.
21. O. POPA, *The extension of circle theorem to the Cauchy integral representation of holomorphic functions*, Bulletin IPT, **15**, *29*, part 1, 1970.
22. O. POPA, *Fluid Mecanics* (in Romanian), **I**/**II**, Tempus Publising House, Timisoara, 2007.
23. FLUENT INC., *FLUENT 6.3 User's Guide*, Lebanon, NH, 2006.
24. ANSYS INC., *ANSYS/FLUENT 16.2 User's Guide*, Canonsburg, PA, 2015.
25. S. DĂNĂILĂ, C. BERBENTE, *Numerical methods in fluid dynamics* (in Romanian), Romanian Academy Publishing House, Bucharest, 2003.
26. D.C. WILCOX, *Formulation of the k-ω turbulence model revisited*, AIAA Journal, **46**, *11*, pp. 2823-2838, 2008.

Received February 28, 2019